HHS Public Access

Author manuscript

Neurodegener Dis. Author manuscript; available in PMC 2016 March 21.

Published in final edited form as:

Neurodegener Dis. 2013 ; 12(1): 23–35. doi:10.1159/000339528.

Consistent Neurodegeneration and Its Association with Clinical Progression in Huntington's Disease: A Coordinate-Based Meta-Analysis

Imis Dogan[#a,b,c], **Simon B. Eickhoff**[#b,d], **Jörg B. Schulz**[a,c], **N. Jon Shah**[a,b,c], **Angela R. Laird**[e], **Peter T. Fox**[e], and **Kathrin Reetz**[a,b,c]

[a] Department of Neurology, RWTH Aachen University, Aachen

[b] Institute of Neuroscience and Medicine, Research Center Jülich GmbH, Jülich

[c] Translational Brain Medicine, Jülich Aachen Research Alliance, Jülich

[d] Institute of Clinical Neuroscience and Medical Psychology, Heinrich Heine University, Düsseldorf , Germany

[e] Research Imaging Center, University of Texas Health Science Center San Antonio, San Antonio, Tex. , USA

[#] These authors contributed equally to this work.

Abstract

Background—The neuropathological hallmark of Huntington's disease (HD) is progressive striatal loss starting several years prior to clinical onset. In the past decade, whole-brain magnetic resonance imaging (MRI) studies have provided accumulating evidence for widely distributed cortical and subcortical atrophy in the early course of the disease.

Objective—In order to synthesize current morphometric MRI findings and to investigate the impact of clinical and genetic features on structural changes, we performed a coordinate-based meta-analysis of voxel-based morphometry (VBM) studies in HD.

Methods—Twenty HD samples derived from 17 studies were integrated in the analysis comparing a total of 685 HD mutation carriers [345 presymptomatic (pre-HD) and 340 symptomatic (symp-HD) subjects] and 507 controls. Convergent findings across studies were delineated using the anatomical likelihood estimation approach. Effects of genetic and clinical parameters on the likelihood of observing VBM findings were calculated by means of correlation analyses.

Results—Pre-HD studies featured convergent evidence for neurodegeneration in the basal ganglia, amygdala, thalamus, insula and occipital regions. In symp-HD, cerebral atrophy was more pronounced and spread to cortical regions (i.e. inferior frontal, premotor, sensorimotor, midcingulate, frontoparietal and temporoparietal cortices). Higher cytosine-adenosine-guanosine

Kathrin Reetz, MD, Department of Neurology, RWTH Aachen University, Pauwelsstrasse 30, DE–52074 Aachen (Germany), Tel. +49 241 80 80283, kreetz@ukaachen.de.

repeats were associated with striatal degeneration, while parameters of disease progression and motor impairment additionally correlated with cortical atrophy, especially in sensorimotor areas.

Conclusion—This first quantitative meta-analysis in HD demonstrates the extent of striatal atrophy and further consistent extrastriatal degeneration before clinical conversion. Sensorimotor areas seem to be core regions affected in symp-HD and, along with widespread cortical atrophy, may account for the clinical heterogeneity in HD.

Keywords

Huntington's disease; Atrophy; Neurodegeneration; Voxel-based morphometry; Anatomical likelihood estimation; Meta-analysis

Introduction

Huntington's disease (HD) is a rare autosomal dominantly inherited neurodegenerative disorder caused by an expanded trinucleotide repeat (cytosine-adenosineguanosine, CAG) located on chromosome 4p encoding the protein huntingtin [1]. Symptom manifestation includes involuntary movements (e.g. chorea) and neuropsychiatric disturbances, usually occurring during mid-adulthood. The neuroanatomical hallmark of HD is degeneration of the striatum starting several years prior to symptom manifestation [2, 3]. Importantly, the neuropathology of HD is not limited to the striatum, and several neuroimaging studies have indicated that extrastriatal subcortical and cortical structures are affected in the early course of the disease (for a review, see Bohanna et al. [4]). Whereas most of the previous in vivo volumetric studies using magnetic resonance imaging (MRI) have concentrated on alterations in predefined brain regions, particularly in the striatum or basal ganglia, in the past decade structural MRI studies have made use of improving MRI acquisition and analysis methods to assess whole-brain changes and to investigate the distribution of structural changes in both symptomatic (symp-HD) and presymptomatic HD (pre-HD). In particular, data from large-scale multinational HD projects (PREDICT-HD [5] , TRACK-HD [6]) have provided new insights into early neurodegenerative processes in HD in order to identify potential biomarkers for disease-modifying trials. Nevertheless, cross-sectional findings of smaller data sets are inconsistent regarding the pattern and extent of neurostructural changes prior to and early after clinical conversion. For instance, findings on volume loss in the pallidum and thalamus in pre-HD have been controversial [7–9], and while most studies indicate that cortical atrophy primarily emerges after symptom onset, others found alterations in frontal, temporal and parietal areas in pre-HD [10, 11]. These discrepancies may be due to methodological differences between studies, or simply because HD is a heterogeneous disorder. Quantitative meta-analysis techniques for neuroimaging data, like the anatomical likelihood estimation (ALE) approach, are well established to search for locations of agreement among significant effects throughout the brain. However, to date there have been no attempts at statistical integrations of accumulating neuroimaging data in HD research. As voxel-based morphometry (VBM) [12] has recently emerged as the technique of choice allowing for observer-independent detection of morphological changes throughout the entire brain on a voxel-wise basis without any regional a priori assumptions,

the growing number of VBM studies on HD now facilitates a meta-analytical integration of their findings to identify core regions affected in pre-HD and symp-HD.

Using the ALE approach, we performed a coordinate-based meta-analysis of VBM studies comparing HD mutation carriers with healthy controls. Our aims were (1) to provide an objective synthesis of the current literature on whole-brain structure changes in HD and to elucidate consistent patterns across studies, (2) to contrast morphometric changes reported in studies on pre-HD subjects with those reported for symp-HD and (3) to investigate the influence of genetic and clinical parameters on the likelihood of observing significantly different findings between HD subjects and controls. Given the partly conflicting findings in the current literature, we expected to find converging striatal atrophy in symp-HD as well as pre-HD and more widespread cortical alterations after clinical conversion, which would be associated with markers of disease progression.

Methods

Literature Search and Study Selection

A systematic search for morphometric studies investigating HD subjects was carried out within the PubMed (http://www.ncbi.nlm.nih.gov/pubmed/) and BrainMap databases (http://brainmap.org/). We further searched the reference lists of published reviews on HD as well as all studies obtained to identify additional studies that were not retrieved in the initial database searches. Studies were selected according to the following criteria:

(1) We only considered studies where whole-brain VBM analyses of MRI data sets were employed to investigate regional volume changes.

(2) The analysis included a direct comparison of genetically confirmed HD subjects and a group of age-matched healthy controls.

(3) Stereotactic whole-brain coordinates were reported in a standardized reference space (Talairach or Montreal Neurological Institute space) for the location of all significant structural differences between HD subjects and controls. For publications that were otherwise suitable for meta-analysis but did not report whole-brain coordinates, the corresponding authors were contacted for additional information, resulting in the inclusion of a further 6 studies [6, 13–17].

(4) To avoid the possibility of nonindependent observations in cases of substantially overlapping samples between studies, only those publications with the larger group size or more detailed information on the sample (e.g. whole-brain coordinates, clinical data) were included.

Thirty publications reporting the usage of VBM were initially considered for the meta-analysis, of which 17 met our inclusion criteria [6, 13–28]. VBM coordinates for the TRACK-HD sample [6] were provided for 4 independent groups (2 pre-HD, 2 symp-HD). From the PREDICT-HD study [5], we included a sample published in Klöppel et al. [14]. Thus, our analysis integrated 20 HD samples and included a total of 685 HD mutation carriers (345 pre-HD, 340 symp-HD) and 507 healthy controls (table 1). Nine samples

included only pre-HD subjects (a total of 337), a further 9 included only symp-HD patients (287) and 2 publications reported pooled cohorts with pre-HD and symp-HD subjects. As far as reported, the large majority of the symptomatic patients (at least 92%) were in an early disease stage based on the total functional capacity score of the Unified Huntington Disease Rating Scale (UHDRS), in which patients' functional capacity to deal with daily routine tasks is intact or mildly impaired (total functional capacity ≥7; stages I and II according to the classification of Shoulson and Fahn [29]). This clinical staging scheme assesses 5 levels of function in the domains of workplace, finances, domestic chores, activities of daily living and requirements for unskilled or skilled care. All of the articles reported gray matter decreases in HD (in total 318 foci), while only 4 studies [6, 18, 24, 25] also reported white matter reductions (32 foci). We therefore focused our analyses on gray matter changes in HD. In none of these studies were significant volume increases found in HD subjects compared to controls. This meta-analysis was performed according to the ethical standards recommended by the Helsinki Declaration.

ALE Algorithm

A revised version [30] of the ALE approach for coordinate-based meta-analysis of neuroimaging data [31–35] was used to test for significant convergence of VBM findings in HD. The ALE algorithm assesses the overlap between foci reported in the individual studies by modeling them as 3-dimensional Gaussian probability distributions centered at the respective coordinates, which accommodate the spatial uncertainty associated with each single focus (e.g. due to between-subject or between-template variance). The algorithm first combined the modeled probabilities of all foci reported in a given study for each voxel. This resulted in a 'modeled anatomical effect' map for each study indicating at each location the probability that a significant difference was located at that position. ALE scores describing the convergence of findings across different studies were then calculated on a voxel-by-voxel basis by taking the union of these individual modeled anatomical effect maps. To enable spatial inference on these 'experimental' ALE scores, an empirical null distribution was derived from a permutation procedure [30], providing a distribution of ALE scores that would be expected under a random spatial association between studies. The null hypothesis thus reflects the lack of any true convergence between studies. To distinguish random convergence from true convergence, the meta-analytically computed ALE scores were then tested against the ALE scores obtained under this null hypothesis at a cluster-level corrected threshold of $p < 0.05$ (cluster-forming threshold at voxel level: $p < 0.001$). Cluster thresholds were derived using a Monte Carlo analysis by randomly redistributing the foci of the individual studies throughout the gray matter of the reference space (according to the International Consortium for Brain Mapping tissue probability maps). Modeled anatomical effect maps were computed for these simulated experiments, followed by ALE calculation and statistical thresholding at the voxel level. The size of the ensuing clusters was recorded, and the procedure was repeated 5,000 times. Cluster-level correction was achieved by retaining only those clusters from the original analysis that were exceeded in size by only 5% of the clusters obtained through the simulation. We performed 3 separate meta-analyses. One analysis was carried out across all 20 HD samples to evaluate disease-related brain structure changes. To investigate anatomic differences between pre-HD and symp-HD, we created separate ALE maps for each study group (each including 9 samples). Additionally,

we used the conservative minimum statistic approach [36] and performed conjunction analysis between these 2 meta-analyses to identify the intersection of regions that are consistently found to be atrophic in pre-HD and symp-HD [37]. Contrast analyses were calculated by means of ALE subtraction analysis (i.e. symp-HD > pre-HD, pre-HD > symp-HD) [37]. This analysis evaluates the difference between the ALE maps obtained for the two groups using a full-relabeling randomization procedure. Confidence estimates, indicating that the difference is indeed due to true group differences rather than sampling, were thresholded at a 95% confidence in true differences to determine regions where the likelihood of finding atrophy was significantly different between pre-HD and symp-HD. The resulting significant anatomical areas were labeled by reference to probabilistic cytoarchitectonic maps of the human brain using the SPM Anatomy Toolbox v1.8 [38]. With this, a maximum probability map represents a summary of different histological maps and allows attribution of each voxel of the reference space to the most likely cytoarchitectonic area [38].

Correlation Analyses

We further tested the dependence of the likelihood of morphometric changes on HD genetic and clinical parameters. In particular, we assessed separately for each of the significant clusters derived from the ALE map across all HD samples, whether the contribution of each study to this cluster was dependent on these covariates. Analysis of genetic load effects (mean CAG repeats) on the likelihood of observing regional atrophy was based on 19 samples (table 1). Age-related impact on morphometric differences was analyzed across all 20 samples. In 3 articles, age was not exactly matched across groups [6, 20, 26], but potential confounding effects due to normal loss from healthy aging were controlled for by including age as a covariate in the analyses. To assess the burden of pathology in both symp-HD and pre-HD and its effect on the likelihood of observing atrophy, we used the index of disease burden based on the following formula: age × (CAG – 35.5) [39]. This score provides an estimate of pathological burden while taking account of the subject's current age and was shown to correlate strongly with HD-related clinical features [6]. Since most studies did not report mean disease burden scores, we calculated an approximation using study-specific mean age and CAG values [i.e. estimated disease burden = mean age × (mean CAG – 35.5)]. As a marker for estimated disease progression, we used the mean disease duration in years reported in 9 studies. For the pre-HD studies, we employed the inverse mean number for estimated years to clinical onset based on the survival analysis by Langbehn et al. [40], which was reported for 6 samples. On the phenotypical level, we used the mean motor scores of the UHDRS, provided for 18 HD samples. Functional and cognitive scores were not reported in sufficient numbers of studies to be included in our analysis (table 1). Across the studies, mean UHDRS motor scores correlated significantly with age, CAG repeats, estimated disease burden and progression (Pearson's $r = 0.86$, 0.74, 0.93 and 0.91, respectively; $p \leq 0.001$). Estimated disease burden also correlated with age, CAG repeats and estimated disease progression ($r = 0.67$, 0.78 and 0.86, respectively; $p \leq 0.002$), and estimated disease progression correlated with age ($r = 0.78$; $p = 0.001$). Due to the small number of included studies, we could not take account of interdependencies between covariates by means of partial regression analysis and calculated nonparametric Spearman's rank coefficients thresholded at a p value of <0.05.

Results

Significant Convergence of Reported Atrophy in HD Compared to Healthy Controls

Pre-HD Studies—Meta-analysis including only pre-HD subjects revealed 4 significant clusters of converging volume reductions in HD subjects when compared with controls (table 2; fig. 1a). The 2 largest clusters were found in the bilateral striatum (caudate nucleus and putamen). The right-hemispheric cluster extended to the pallidum and centromedial amygdala, adjoining the hippocampus and posterior insula, while the left-hemispheric cluster extended to the anteriormedial thalamus connected to the prefrontal cortex [41]. A further subcortical cluster showed atrophy in the left putamen and amygdala, bordering on the hippocampus and posterior insula. Finally, 1 cluster was located in the right occipital cortex.

Symp-HD Studies—In symp-HD, we found 8 significant clusters (table 2; fig. 1b), with 2 clusters showing convergent bilateral striatal degeneration extending to the pallidum and right nucleus accumbens. Further cortical clusters revealed consistent atrophy bilaterally in the inferior frontal gyrus (overlapping with Broca's area), primary motor cortex (M1), right lateral premotor cortex (PMC), left somatosensory cortex (SI), rostral inferior parietal cortex (IPC) and anterior lateral intraparietal sulcus (IPS). One cluster was located in the right midcingulate cortex extending to the medial PMC (supplementary motor area, SMA), and another left-hemispheric cluster was centered in the parietal operculum (OP4; secondary somatosensory cortex, SII) adjoining Heschl's gyrus and the insular cortex.

All HD Studies—Across all HD studies, we found 6 significant clusters of convergence (table 2; fig. 1c). The 2 largest clusters were centered in the bilateral striatum, extending to the pallidum. The inferior frontal gyrus including Broca's area was also affected bilaterally. One cluster comprised converging volume reductions in the left M1, lateral PMC, SI, IPC and IPS, and another cluster was found in the left middle and superior occipital gyrus including parts of the cuneus and precuneus.

Comparison of Pre-HD and Symp-HD—Conjunction analysis between pre-HD and symp-HD yielded two clusters showing common volume reductions in the bilateral basal ganglia (table 2; fig. 1d). Contrast of symp-HD with pre-HD yielded 9 significant clusters indicating more pronounced and widespread atrophy in the clinical disease stage (symp-HD > pre-HD; table 2; fig. 1e). Differences were detected primarily in cortical regions, i.e. bilaterally in the inferior frontal gyrus (overlapping with Broca's area), motor areas (M1, PMC), left SI, SII, Heschl's gyrus and insular and parietal cortices (IPC, IPS). One cluster was located in the right midcingulate cortex extending to the SMA, and 2 left-hemispheric clusters included parts of the middle and superior occipital gyrus, cuneus and precuneus. Subcortically more pronounced atrophy in symp-HD was found in the right striatum, pallidum and nucleus accumbens. No significant effects were found in the reverse contrast (pre-HD > symp-HD), indicating that there was no region where significant atrophy was more likely to be observed in pre-HD mutation carriers than in symp-HD patients.

Correlation Analyses

A higher likelihood of finding morphometric differences with increasing CAG repeat length was found in the right striatum (table 3; fig. 2). Age-dependent atrophy was observed in 5 clusters, located in the bilateral striatum and further in cortical areas, i.e. the bilateral M1, right PMC and left parietal regions (SI, SII, IPC, IPS). Similar results were obtained on the phenotypical level, as we found 4 significant clusters in nearly the same regions (except for the left striatum), demonstrating an association between higher UHDRS motor scores and the chance of observing volume loss in HD. Correlation analysis with the estimated disease burden score yielded 3 significant clusters. One was located in the right striatum extending to the pallidum, and 2 cortical clusters were found in the bilateral M1, right PMC, left SI and IPC. Dependence of morphometric alterations on our estimated disease progression score was found in the left caudate nucleus and bilateral M1 extending to the right PMC and left SI. For all covariates, Spearman's rank coefficients ranged from 0.47 to 0.56, but the strongest association was shown between the estimated disease burden score and the likelihood of atrophy in the right striatum (Spearman's rank correlation coefficient = 0.62; table 3; fig. 2).

Discussion

To our knowledge, this is the first quantitative meta-analysis of neurostructural changes in HD. Using a coordinate-based ALE meta-analysis, we integrated the VBM results of 20 HD samples comparing a total of 685 HD subjects and 507 controls. Our results demonstrate the brunt of the degenerative process in the striatum and also provide evidence of consistent atrophy extending to the pallidum, amygdala, thalamus and insular and occipital cortices in the prodromal stage. After symptom manifestation, cerebral volume loss extends to several cortical areas, primarily motor and sensorimotor cortices, showing significant correlations with markers of disease progression and motor impairment.

The consistent bilateral striatal degeneration shown in a heterogeneous pre-HD sample with regard to estimated onset roughly up to 2 decades (table 1) is in line with previous studies, which have documented striatal volume loss up to 15 years before clinically diagnosable HD and reductions by as much as half at the time of diagnosis [2, 3, 8]. Though our meta-analytical approach does not permit analysis of when atrophy in the striatum begins, this cross-sectional synthesis of VBM findings reliably depicts the most prominent neuropathological feature in HD. Remarkably, clusters of convergence in the pre-HD analysis were mainly centered in the striatum but further extended to extrastriatal subcortical nuclei and insular and occipital cortices. Due to the progressive nature of the disease, it is surprising that the cytoarchitectonically allocated atrophy in the amygdala, hippocampus and anteromedial thalamus could not be substantiated in the symp-HD analysis or across all HD studies. In a volumetric TRACK-HD analysis investigating the rate of atrophy in subcortical nuclei, Van den Bogaard et al. [9] found volume reductions in the basal ganglia in the pre-HD sample closer to disease onset, whereas the atrophy observed in the thalamus, amygdala and hippocampus did not exceed the overall whole-brain atrophy. In contrast, using VBM, Kassubek et al. [42] reported thalamic atrophy *only* in covariation with cognitive performance in early cognitively impaired HD patients. Hence, we would ascribe this

somewhat inconsistent finding to a less robust effect in these regions, most likely depending on selective patient characteristics, though they seem to be a critical part of incipient degeneration processes in HD. This is supported by our ALE subtraction analysis performed at a more lenient threshold but showing no significant differences between the two study groups in these subcortical nuclei.

The topography of brain atrophy in symp-HD demonstrates progression of neurodegeneration from predominantly subcortical to more widespread cortical atrophy related to clinical conversion. Interestingly, consistent cortical degeneration was primarily found in regions forming the motor loop, which connects the putamen with motor and sensorimotor areas (i.e. PMC, SMA, M1, SI). This finding in mostly early HD patients is consistent with previous research on cortical thinning showing the most marked changes in the sensorimotor cortex in early HD patients [43] and the suggestion of selective vulnerability in motor pathways in HD [44]. Since clinical onset in HD is conventionally defined by the presence of motor symptoms, it is reasonable that motor areas are core regions affected in symp-HD. However, impairments of voluntary movement control are often ascribed to degeneration of the striatum and striatal pathways, whilst there is evidence of cortical contribution to HD's phenotype independent of striatal connectivity [43]. This is supported by the results of our regression analysis performed with mean UHDRS motor scores, which primarily yielded significant clusters in cortical areas underlying motor functioning rather than in the striatum. Moreover, in a recent functional connectivity analysis of frontoparietal regions, OP4 within the parietal operculum was strongly connected to the PMC and M1 and associated with sensorimotor processing and action control (i.e. motor-related tasks) [45], regions found to be atrophic in HD patients exhibiting motor signs and covarying with motor impairment.

Our observed pattern of cortical degeneration in symp-HD further included regions beyond motor areas and might be related to the clinical heterogeneity in symp-HD. Atrophy in prefrontal and parietal cortices along with the early degeneration of the caudate nucleus may lead to deficits in attention, working memory and executive functioning via disruptions of cognitive basal ganglia-thalamocortical loops [46]. Volume reductions in the cingulate have been associated with impaired visual working memory, recognition of negative emotions and mood symptomatology in HD, both in vivo [47] and in postmortem studies [48]. Another connectivity analysis revealed a core network underlying overt speech production and consisting of Broca's area, the insula, basal ganglia, cerebellum, PMC and M1 [49], dysfunctions of which may underlie dysarthria in HD. We further found consistent atrophy in the inferior parietal cortex and intraparietal sulcus, playing an important role in higher cognitive functioning and somatosensory and visuomotor integration [50]. For instance, Rupp et al. [51] reported significant associations between degeneration in the left inferior parietal lobule and antisaccade in HD, an important phenotypical feature in HD. Finally, volume reductions in the insula were associated with emotion processing deficits in HD, especially for the recognition of disgust, which is already detectable before symptom onset [52]. In summary, we conclude that extrastriatal subcortical and insular degenerations are evident in the course of HD's prodrome, which might, in addition to striatal degeneration, constitute early subtle changes seen in pre-HD. Alterations in predominantly motor areas and further in the frontal, parietal, temporoparietal and midcingulate cortices found in the

manifest disease stage may be secondary to these and contribute to the clinical heterogenity in HD.

Research on the role of genetic markers as a determinant of structural degeneration in HD has yielded disparate results, with some studies demonstrating an impact of genetic load on striatal and extrastriatal atrophy [19, 20], in cortical but not subcortical regions [26], and, by contrast, some studies not detecting any correlations at all [7, 13]. In our analysis, effects of higher CAG repeats on morphometric differences between HD subjects and controls were shown in the right striatum, which might be ascribed to a lack of variance since we only included mean CAG repeats for each study without accounting for relative dispersions within samples. However, given the evidence that CAG repeat length is inversely correlated with age of onset [40], our results imply that genetic load plays a decisive role in early striatal degeneration, determining the onset of first symptom outbursts, but may have no incremental impact on cortical changes seen in later stages. This is in agreement with a recent study reporting a significant relationship between CAG repeats and cross-sectional caudate volumes at baseline, but not for the rate of volume loss at the 1-year follow-up [53]. Age-dependent morphometric changes were observed in striatal and cortical regions distinctive of the symptomatic stage. Though we could not control for age of onset, this finding seems to mirror the progressive nature of HD related to clinical conversion, as age was either matched or controlled for as a covariate in the respective studies. Considering both age and CAG repeats, we computed an approximation of the disease burden pathology and found significant associations with atrophy in the striatum and sensorimotor cortex. The association with striatal loss was stronger than for any other covariate but was restricted to the right striatum, which might be due to our approximated version of the score calculated by study-specific mean values without taking account of variances within samples. Nevertheless, as the burden of pathology score represents an interaction term between age and CAG repeats [6, 39] and therefore considers both a genetic and disease progression factor, our analysis confirms that it reliably depicts early subcortical as well as motor-related degeneration features in HD. Finally, analysis with our estimated disease progression score based on disease duration in symp-HD and predicted time to onset in pre-HD showed associations again with sensorimotor and left caudate atrophy. It has been suggested that a surplus of synaptic activity in the dominant left hemisphere might aggravate differential oxidative stress and cause leftward-biased striatal atrophy in HD [54]. This notion accords with the leftward-biased caudate atrophy associated with the exposure to HD's neurotoxicity – as expressed in our disease progression score – but needs to be addressed in targeted asymmetry analyses, since the majority of included studies did not report any information on handedness.

As with any meta-analytical approach, the applied ALE algorithm is based on the data provided by the primary articles. Since there is no absolute standard VBM procedure, methodological differences within studies (e.g. preprocessing steps, smoothing kernel, statistical threshold) may add to divergent study results, underlining the need for a meta-analytical integration. Consequently, there have been neuroimaging studies reporting atrophic regions in HD that were not confirmed in our analysis (e.g. hypothalamus, cerebellum, substantia nigra). Effects in these regions might be relatively weak or rather inconsistent across different patient populations and therefore not represented in our meta-

analysis. It is also possible that the varying coverage of reported foci in the original studies (i.e. cluster maxima versus separate maxima within a cluster) might have contributed to spatial biases, whereby larger clusters in particular could not be depicted accurately. Further, note that each correlation analysis was based on study-inherent mean scores, whereas variances of values within studies were not taken into account. This might have delimited differential aspects of covariance between morphometric changes and clinical parameters, particularly for age and years to estimated disease onset, for which standard deviations ranged around 1 decade (table 1). Another important caveat for the interpretation of our regression analysis concerns the intercorrelations between covariates, resulting in a substantial portion of shared variance and overlapping brain areas, especially in the sensorimotor cortex. Since all of our regression parameters are each somewhat a marker of disease progression, the high interdependency is not surprising and rather indicates the prognostic value of extrastriatal regions in monitoring disease progression, particularly considering that each of the covariates seemed to feature differential aspects of corticostriatal alterations. It might have been interesting to investigate associations of observed atrophy with other phenotypical features (e.g. cognitive, psychiatric), but most VBM studies did not report standardized scores on these domains. Overall, by means of quantitative meta-analysis, we tried to overcome study-specific idiosyncrasies and identified characteristic anatomical regions showing converging evidence for HD-related neurodegeneration. Importantly, significant clusters in a meta-analysis are yielded if convergence across studies occurs more likely than expected by chance, even though this does not require all or even the majority of the studies to show alterations in those particular regions [32]. Using a meta-analytical approach, we provided an objective modeling of spatial uncertainty relative to individual sample sizes and testing for convergence across different neuroimaging studies on HD. Future studies reporting more detailed information on sample characteristics and imaging results will allow validation of our findings and facilitate further meta-analyses on other morphometric or multimodal neuroimaging approaches as promising tools to elucidate the complexity of the neuropathology of HD.

Conclusions

This first quantitative meta-analysis in HD, including a total of 685 mutation carriers, provides an objective evaluation of brain structure changes in this rare neurodegenerative disorder. Our results demonstrate that extrastriatal atrophy is indeed consistently present in the presymptomatic stage, signifying that it might occur parallel to initial striatal atrophy. After symptom manifestation, atrophy is more pronounced and widespread, with sensorimotor areas as core regions affected in the symptomatic stage. This was highlighted by regression analyses outlining the impact of genetic load on early subcortical atrophy, and associations between clinical disease progression and advanced cortical alterations, especially in the sensorimotor cortex. Our data condense the current VBM literature in HD and provide evidence of consistent extrastriatal subcortical and cortical parametric changes in a disease prominent for its clinical heterogeneity. This underlines the need to extend the focus of research from the key region of neuropathology to a more differentiated picture of cortical-subcortical changes from early on and potential disturbances in the networks formed by these regions.

Acknowledgements

We would like to thank all contacted authors for their valuable input in this study, especially Dr. Rachael Scahill for providing the TRACK-HD VBM data. P.T.F., A.R.L. and S.B.E. were funded by the Human Brain Project (R01-MH074457-01A1). S.B.E. also acknowledges funding by the Initiative and Networking Fund of the Helmholtz Association within the Helmholtz Alliance on Systems Biology (Human Brain Model) and the International Research Training Group 1328. S.B.E. and K.R. were funded by the Deutsche Forschungsgemeinschaft Translational Brain Research in Psychiatry and Neurology (DFG ZUK32/1).

References

1. The Huntington's Disease Collaborative Research Group. A novel gene containing a tri-nucleotide repeat that is expanded and unstable on Huntington's disease chromosomes. Cell. 1993; 72:971–983. [PubMed: 8458085]
2. Aylward EH, Sparks BF, Field KM, Yallapragada V, Shpritz BD, Rosenblatt A, Brandt J, Gourley LM, Liang K, Zhou H, Margolis RL, Ross CA. Onset and rate of striatal atrophy in preclinical Huntington disease. Neurology. 2004; 63:66–72. [PubMed: 15249612]
3. Paulsen JS, Nopoulos PC, Aylward E, Ross CA, Johnson H, Magnotta VA, Juhl A, Pierson RK, Mills J, Langbehn D, Nance M. PREDICT-HD Investigators and Coordinators of the Huntington's Study Group (HSG): Striatal and white matter predictors of estimated diagnosis for Huntington disease. Brain Res Bull. 2010; 82:201–207. [PubMed: 20385209]
4. Bohanna I, Georgiou-Karistianis N, Hannan AJ, Egan GF. Magnetic resonance imaging as an approach towards identifying neuro-pathological biomarkers for Huntington's disease. Brain Res Rev. 2008; 58:209–225. [PubMed: 18486229]
5. Paulsen JS, Hayden M, Stout JC, Langbehn DR, Aylward E, Ross CA, Guttman M, Nance M, Kieburtz K, Oakes D, Shoulson I, Kayson E, Johnson S, Penziner E. Preparing for preventive clinical trials: the Predict-HD study. Arch Neurol. 2006; 63:883–890. [PubMed: 16769871]
6. Tabrizi SJ, Langbehn DR, Leavitt BR, Roos RA, Durr A, Craufurd D, Kennard C, Hicks SL, Fox NC, Scahill RI, Borowsky B, Tobin AJ, Rosas HD, Johnson H, Reilmann R, Landwehrmeyer B, Stout JC. Biological and clinical manifestations of Huntington's disease in the longitudinal TRACK-HD study: cross-sectional analysis of baseline data. Lancet Neurol. 2009; 8:791–801. [PubMed: 19646924]
7. Harris GJ, Codori AM, Lewis RF, Schmidt E, Bedi A, Brandt J. Reduced basal ganglia blood flow and volume in pre-symptomatic, gene-tested persons at-risk for Huntington's disease. Brain. 1999; 122:1667–1678. [PubMed: 10468506]
8. Paulsen JS, Magnotta VA, Mikos AE, Paulson HL, Penziner E, Andreasen NC, Nopoulos PC. Brain structure in preclinical Huntington's disease. Biol Psychiatry. 2006; 59:57–63. [PubMed: 16112655]
9. van den Bogaard SJ, Dumas EM, Acharya TP, Johnson H, Langbehn DR, Scahill RI, Tabrizi SJ, van Buchem MA, van der Grond J, Roos RA. Early atrophy of pallidum and accumbens nucleus in Huntington's disease. J Neurol. 2011; 258:412–420. [PubMed: 20936300]
10. Rosas HD, Hevelone ND, Zaleta AK, Greve DN, Salat DH, Fischl B. Regional cortical thinning in preclinical Huntington disease and its relationship to cognition. Neurology. 2005; 65:745–747. [PubMed: 16157910]
11. Nopoulos PC, Aylward EH, Ross CA, Johnson HJ, Magnotta VA, Juhl AR, Pierson RK, Mills J, Langbehn DR, Paulsen JS. PREDICT-HD Investigators Coordinators of Huntington Study Group (HSG): Cerebral cortex structure in prodromal Huntington disease. Neurobiol Dis. 2010; 40:544–554. [PubMed: 20688164]
12. Ashburner J, Friston KJ. Voxel-based morphometry – the methods. Neuroimage. 2000; 11:805–821. [PubMed: 10860804]
13. Douaud G, Gaura V, Ribeiro MJ, Lethimonnier F, Maroy R, Verny C, Krystkowiak P, Damier P, Bachoud-Levi AC, Hantraye P, Remy P. Distribution of grey matter atrophy in Huntington's disease patients: a combined ROI-based and voxel-based morphometric study. Neuroimage. 2006; 32:1562–1575. [PubMed: 16875847]

14. Klöppel S, Chu C, Tan GC, Draganski B, Johnson H, Paulsen JS, Kienzle W, Tabrizi SJ, Ashburner J, Frackowiak RS. Automatic detection of preclinical neurodegeneration: presymptomatic Huntington disease. Neurology. 2009; 72:426–431. [PubMed: 19188573]
15. Klöppel S, Stonnington CM, Petrovic P, Mobbs D, Tuscher O, Craufurd D, Tabrizi SJ, Frackowiak RS. Irritability in pre-clinical Huntington's disease. Neuropsychologia. 2010; 48:549–557. [PubMed: 19878688]
16. Stoffers D, Sheldon S, Kuperman JM, Goldstein J, Corey-Bloom J, Aron AR. Contrasting gray and white matter changes in pre-clinical Huntington disease: an MRI study. Neurology. 2010; 74:1208–1216. [PubMed: 20385893]
17. Wolf RC, Vasic N, Schonfeldt-Lecuona C, Landwehrmeyer GB, Ecker D. Dorsolateral prefrontal cortex dysfunction in presymptomatic Huntington's disease: evidence from event-related fMRI. Brain. 2007; 130:2845–2857. [PubMed: 17855375]
18. Gavazzi C, Nave RD, Petralli R, Rocca MA, Guerrini L, Tessa C, Diciotti S, Filippi M, Piacentini S, Mascalchi M. Combining functional and structural brain magnetic resonance imaging in Huntington disease. J Comput Assist Tomogr. 2007; 31:574–580. [PubMed: 17882035]
19. Gomez-Anson B, Alegret M, Munoz E, Monte GC, Alayrach E, Sanchez A, Boada M, Tolosa E. Prefrontal cortex volume reduction on MRI in preclinical Huntington's disease relates to visuomotor performance and CAG number. Parkinsonism Relat Disord. 2009; 15:213–219. [PubMed: 18632301]
20. Henley SM, Wild EJ, Hobbs NZ, Scahill RI, Ridgway GR, Macmanus DG, Barker RA, Fox NC, Tabrizi SJ. Relationship between CAG repeat length and brain volume in pre-manifest and early Huntington's disease. J Neurol. 2009; 256:203–212. [PubMed: 19266143]
21. Ille R, Schafer A, Scharmuller W, Enzinger C, Schoggl H, Kapfhammer HP, Schienle A. Emotion recognition and experience in Huntington disease: a voxel-based morphometry study. J Psychiatry Neurosci. 2011; 36:383–390. [PubMed: 21406159]
22. Kassubek J, Juengling FD, Kioschies T, Henkel K, Karitzky J, Kramer B, Ecker D, Andrich J, Saft C, Kraus P, Aschoff AJ, Ludolph AC, Landwehrmeyer GB. Topography of cerebral atrophy in early Huntington's disease: a voxel based morphometric MRI study. J Neurol Neurosurg Psychiatry. 2004; 75:213–220. [PubMed: 14742591]
23. Mühlau M, Weindl A, Wohlschlager AM, Gaser C, Stadtler M, Valet M, Zimmer C, Kassubek J, Peinemann A. Voxel-based morphometry indicates relative preservation of the limbic prefrontal cortex in early Huntington disease. J Neural Transm. 2007; 114:367–372. [PubMed: 17024326]
24. Nave RD, Ginestroni A, Tessa C, Giannelli M, Piacentini S, Filippi M, Mascalchi M. Regional distribution and clinical correlates of white matter structural damage in Huntington disease: a tract-based spatial statistics study. AJNR Am J Neuroradiol. 2010; 31:1675–1681. [PubMed: 20488902]
25. Peinemann A, Schuller S, Pohl C, Jahn T, Weindl A, Kassubek J. Executive dysfunction in early stages of Huntington's disease is associated with striatal and insular atrophy: a neuropsychological and voxel-based morphometric study. J Neurol Sci. 2005; 239:11–19. [PubMed: 16185716]
26. Thieben MJ, Duggins AJ, Good CD, Gomes L, Mahant N, Richards F, McCusker E, Frackowiak RS. The distribution of structural neuropathology in pre-clinical Huntington's disease. Brain. 2002; 125:1815–1828. [PubMed: 12135972]
27. Wolf RC, Vasic N, Schonfeldt-Lecuona C, Ecker D, Landwehrmeyer GB. Cortical dys-function in patients with Huntington's disease during working memory performance. Hum Brain Mapp. 2009; 30:327–339. [PubMed: 18172852]
28. Zimbelman JL, Paulsen JS, Mikos A, Reynolds NC, Hoffmann RG, Rao SM. fMRI detection of early neural dysfunction in pre-clinical Huntington's disease. J Int Neuropsychol Soc. 2007; 13:758–769. [PubMed: 17697407]
29. Shoulson I, Fahn S. Huntington disease: clinical care and evaluation. Neurology. 1979; 29:1–3. [PubMed: 154626]
30. Eickhoff SB, Laird AR, Grefkes C, Wang LE, Zilles K, Fox PT. Coordinate-based activation likelihood estimation meta-analysis of neuroimaging data: a random-effects approach based on empirical estimates of spatial uncertainty. Hum Brain Mapp. 2009; 30:2907–2926. [PubMed: 19172646]

31. Turkeltaub PE, Eden GF, Jones KM, Zeffiro TA. Meta-analysis of the functional neuro-anatomy of single-word reading: method and validation. Neuroimage. 2002; 16:765–780. [PubMed: 12169260]
32. Turkeltaub PE, Eickhoff SB, Laird AR, Fox M, Wiener M, Fox P. Minimizing within-experiment and within-group effects in activation likelihood estimation meta-analyses. Hum Brain Mapp. 2012; 33:1–13. [PubMed: 21305667]
33. Schroeter ML, Raczka K, Neumann J, Yves von Cramon D. Towards a nosology for frontotemporal lobar degenerations – a meta-analysis involving 267 subjects. Neuroimage. 2007; 36:497–510. [PubMed: 17478101]
34. Schroeter ML, Raczka K, Neumann J, von Cramon DY. Neural networks in frontotemporal dementia – a meta-analysis. Neurobiol Aging. 2008; 29:418–426. [PubMed: 17140704]
35. Glahn DC, Laird AR, Ellison-Wright I, Thelen SM, Robinson JL, Lancaster JL, Bullmore E, Fox PT. Meta-analysis of gray matter anomalies in schizophrenia: application of anatomic likelihood estimation and network analysis. Biol Psychiatry. 2008; 64:774–781. [PubMed: 18486104]
36. Nichols T, Brett M, Andersson J, Wager T, Poline JB. Valid conjunction inference with the minimum statistic. Neuroimage. 2005; 25:653–660. [PubMed: 15808966]
37. Caspers S, Zilles K, Laird AR, Eickhoff SB. ALE meta-analysis of action observation and imitation in the human brain. Neuroimage. 2010; 50:1148–1167. [PubMed: 20056149]
38. Eickhoff SB, Stephan KE, Mohlberg H, Grefkes C, Fink GR, Amunts K, Zilles K. A new SPM toolbox for combining probabilistic cytoarchitectonic maps and functional imaging data. Neuroimage. 2005; 25:1325–1335. [PubMed: 15850749]
39. Penney JB Jr, Vonsattel JP, MacDonald ME, Gusella JF, Myers RH. CAG repeat number governs the development rate of pathology in Huntington's disease. Ann Neurol. 1997; 41:689–692. [PubMed: 9153534]
40. Langbehn DR, Brinkman RR, Falush D, Paulsen JS, Hayden MR. A new model for prediction of the age of onset and penetrance for Huntington's disease based on CAG length. Clin Genet. 2004; 65:267–277. [PubMed: 15025718]
41. Behrens TE, Johansen-Berg H, Woolrich MW, Smith SM, Wheeler-Kingshott CA, Boulby PA, Barker GJ, Sillery EL, Sheehan K, Ciccarelli O, Thompson AJ, Brady JM, Matthews PM. Non-invasive mapping of connections between human thalamus and cortex using diffusion imaging. Nat Neurosci. 2003; 6:750–757. [PubMed: 12808459]
42. Kassubek J, Juengling FD, Ecker D, Land-wehrmeyer GB. Thalamic atrophy in Huntington's disease co-varies with cognitive performance: a morphometric MRI analysis. Cereb Cortex. 2005; 15:846–853. [PubMed: 15459079]
43. Rosas HD, Salat DH, Lee SY, Zaleta AK, Pappu V, Fischl B, Greve D, Hevelone N, Hersch SM. Cerebral cortex and the clinical expression of Huntington's disease: complexity and heterogeneity. Brain. 2008; 131:1057–1068. [PubMed: 18337273]
44. Bohanna I, Georgiou-Karistianis N, Egan GF. Connectivity-based segmentation of the striatum in Huntington's disease: vulnerability of motor pathways. Neurobiol Dis. 2011; 42:475–481. [PubMed: 21382492]
45. Eickhoff SB, Jbabdi S, Caspers S, Laird AR, Fox PT, Zilles K, Behrens TE. Anatomical and functional connectivity of cytoarchitec-tonic areas within the human parietal operculum. J Neurosci. 2010; 30:6409–6421. [PubMed: 20445067]
46. Alexander GE, DeLong MR, Strick PL. Parallel organization of functionally segregated circuits linking basal ganglia and cortex. Annu Rev Neurosci. 1986; 9:357–381. [PubMed: 3085570]
47. Hobbs NZ, Pedrick AV, Say MJ, Frost C, Dar Santos R, Coleman A, Sturrock A, Craufurd D, Stout JC, Leavitt BR, Barnes J, Tabrizi SJ, Scahill RI. The structural involvement of the cingulate cortex in premanifest and early Huntington's disease. Mov Disord. 2011; 26:1684–1690. [PubMed: 21557312]
48. Thu DC, Oorschot DE, Tippett LJ, Nana AL, Hogg VM, Synek BJ, Luthi-Carter R, Wald-vogel HJ, Faull RL. Cell loss in the motor and cingulate cortex correlates with symptom-atology in Huntington's disease. Brain. 2010; 133:1094–1110. [PubMed: 20375136]
49. Eickhoff SB, Heim S, Zilles K, Amunts K. A systems perspective on the effective connectivity of overt speech production. Philos Transact A Math Phys Eng Sci. 2009; 367:2399–2421.

50. Culham JC, Cavina-Pratesi C, Singhal A. The role of parietal cortex in visuomotor control: what have we learned from neuro-imaging? Neuropsychologia. 2006; 44:2668–2684. [PubMed: 16337974]

51. Rupp J, Dzemidzic M, Blekher T, West J, Hui S, Wojcieszek J, Saykin AJ, Kareken DA, Foroud T. Comparison of vertical and horizontal saccade measures and their relation to gray matter changes in premanifest and manifest Huntington disease. J Neurol. 2012; 259:267–276. [PubMed: 21850389]

52. Kipps CM, Duggins AJ, McCusker EA, Calder AJ. Disgust and happiness recognition correlate with anteroventral insula and amygdala volume respectively in preclinical Huntington's disease. J Cogn Neurosci. 2007; 19:1206–1217. [PubMed: 17583995]

53. Rosas HD, Reuter M, Doros G, Lee SY, Triggs T, Malarick K, Fischl B, Salat DH, Hersch SM. A tale of two factors: what determines the rate of progression in Huntington's disease? A longitudinal MRI study. Mov Disord. 2011; 26:1691–1697. [PubMed: 21611979]

54. Mühlau M, Gaser C, Wohlschlager AM, Weindl A, Stadtler M, Valet M, Zimmer C, Kassubek J, Peinemann A. Striatal gray matter loss in Huntington's disease is leftward biased. Mov Disord. 2007; 22:1169–1173. [PubMed: 17394246]

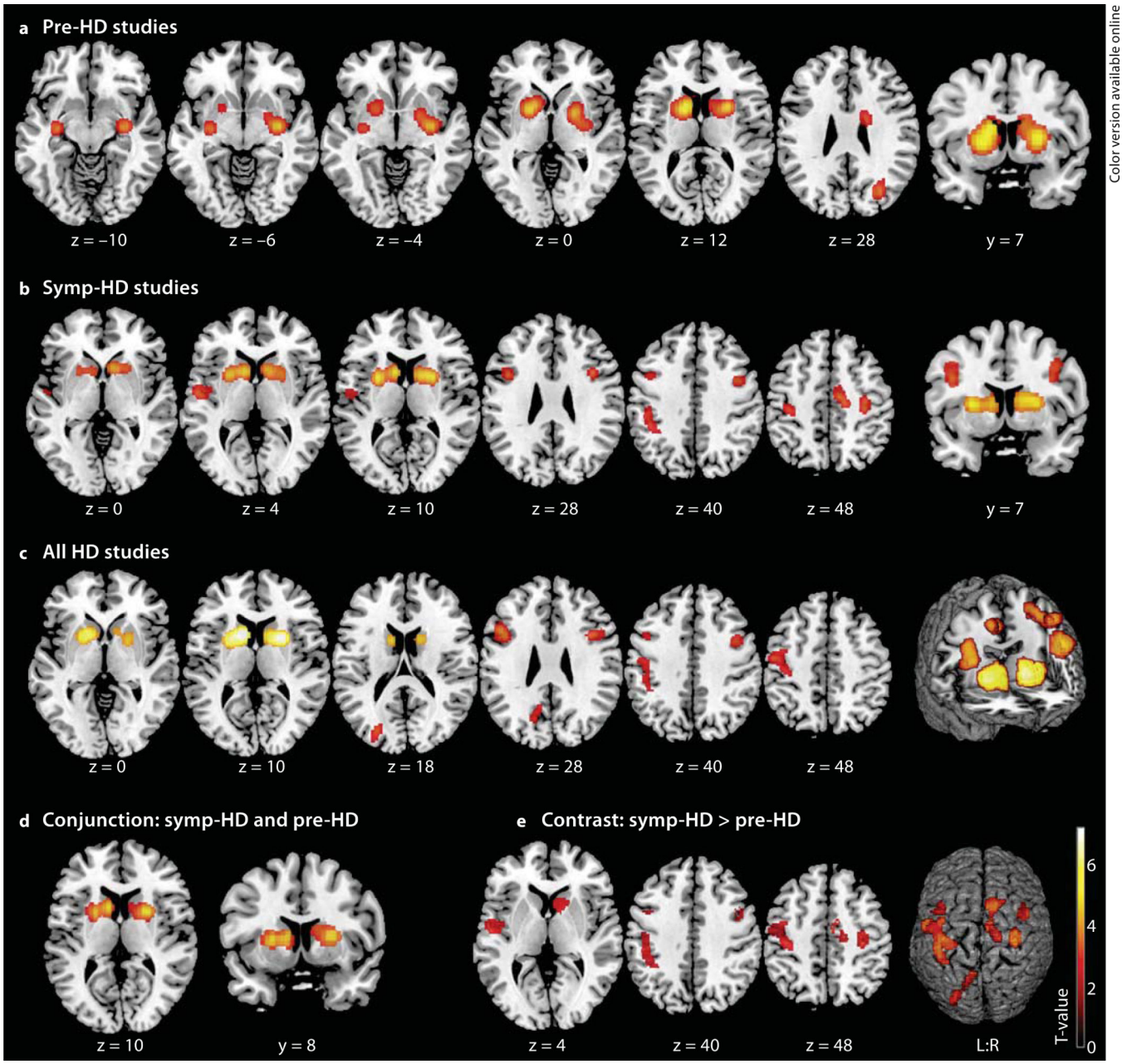

Fig. 1.

Significant clusters from ALE meta-analyses displayed on a template brain (coordinates in Montreal Neurological Institute space, left is left). **a** Regions of volume loss in pre-HD subjects compared to controls were located in the bilateral striatum extending to the amygdala, hippocampus, right pallidum, posterior insula, occipital cortex and left thalamus. **b** Volume loss in symp-HD studies was observed in bilateral basal ganglia, inferior frontal gyrus and motor cortices (PMC, M1), extending to the left somatosensory cortex (SI, SII), parietal areas (IPC, IPS), insula and right midcingulate cortex. **c** Atrophy across all HD studies was detected in the same areas, except for the right motor cortex and left SII, and was additionally observed in left occipitoparietal areas. **d** Conjunction analysis. Common

atrophy in pre-HD and symp-HD was found in the bilateral basal ganglia. **e** Contrast analysis. More pronounced atrophy in symp-HD compared to pre-HD was found in the right basal ganglia, bilateral inferior frontal gyrus and motor cortex, left somatosensory, parietal and occipital areas, insula and right midcingulate cortex.

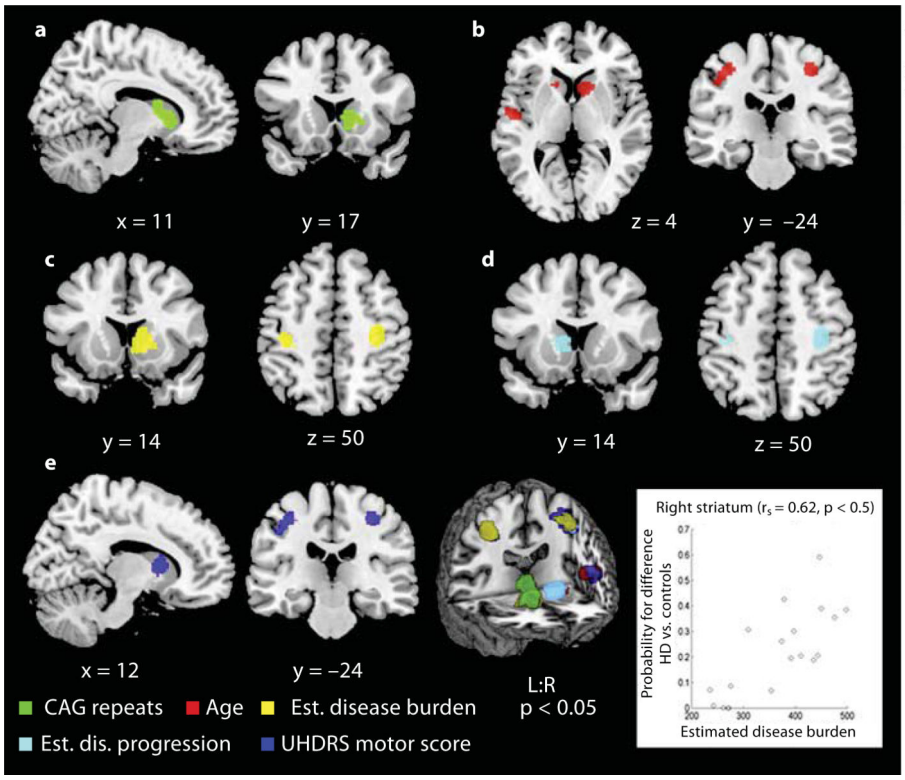

Fig. 2.

Significant clusters of correlation from meta-analyses displayed on a template brain (coordinates in Montreal Neurological Institute space, left is left). The likelihood of observing volume differences between HD subjects and controls covaried with study-specific parameters in the following manner: with CAG-repeat length in the right striatum (**a**); with age in the bilateral striatum and motor cortex and left somatosensory (SI, SII) and parietal (IPC, IPS) regions (**b**); with estimated disease burden in the right basal ganglia and bilateral motor cortex extending to the left SI and IPC (**c**); with estimated disease progression in the left caudate nucleus and bilateral motor cortex extending to the left SI (**d**), and with UHDRS motor scores in the right caudate nucleus, bilateral motor cortex and left somatosensory (SI, SII) and parietal (IPC, IPS) regions (**e**). The strongest association was observed between the estimated disease burden score and the likelihood of atrophy in the right striatum (displayed in the scatter plot). r_S = Spearman's rank correlation coefficient.

Table 1

Summary of the articles included in the meta-analysis

No. Authors	Control subjects		HD subjects								GM foci	FWHM mm
	n (male)	age years	n (male)	age years	HD stage	CAG repeats	DD (YEO) years	UHDRS scores				
								TFC	motor	cognitive		
1 Douaud et al. 2006 [13]	12 (7)	41 ± 9	20 (12)	44 ± 8	I, II	45.4 ± 4	5.7 ± 2	-	34.4 ± 12	217.4 ± 69	26	8
2 Gavazzi et al. 2007 [18]	11 (6)	47 ± 10	9 (6)	55.8 ± 11	I, II, III	39-50	8.5	-	41	-	4	10
3 Gomez-Anson et al. 2009 [19]	21 (11)	33.2 ± 9	20 (11)	33 ± 9	pre	43.7 ± 2	-	-	1.96	-	6	10
4 Henley et al. 2009 [20]	20 (7)	44.9 ± 11	40 (20)	48.5 ± 10	I, II[3]	43.7 ± 2	-	10.9 ± 2	28.9 ± 13	231.5 ± 54	27	8
5 Ille et al. 2011 [21]	18 (10)	49.2 ± 10	18 (10)	51.9 ± 10	symp	45.1 ± 3	4 ± 2	9.6 ± 3	31 ± 18	-	9	10
6 Kassubek et al. 2004 [22]	22 (10)	44.1 ± 17	44 (21)	44.7 ± 11	I, II	45.5 ± 8	5.1 ± 3	10.9 ± 1	24.1 ± 12	196.6 ± 63	17	6
7 Klöppel et al. 2009 [14][1]	95 (29)	44.6	96 (28)	41.8	pre	42.9	-	-	-	-	10	8
8 Klöppel et al. 2010 [15]	16 (7)	40.4 ± 9	16 (8)	39.3 ± 8	pre	42.1 ± 2	(16.8 ± 9)	-	2.3 ± 2	-	15	12
9 Mühlau et al. 2007 [23]	46 (23)	44 ± 10	46 (23)	44 ± 11	pre, I, II	44 ± 2	4.7 ± 5	-	18 ± 17	-	32	8
10 Nave et al. 2010 [24]	15 (8)	55 ± 12	15 (8)	56 ± 12	pre, I-III	44 ± 3	6.9 ± 7	-	33 ± 18	-	9	-
11 Peinemann et al. 2005 [25]	25 (13)	42.9 ± 10	25 (13)	43.8 ± 8	I, II	44.1 ± 3	4.7 ± 4	-	15.7 ± 13	-	5	6
12 Stoffers et al. 2010 [16]	25 (9)	39.1 ± 12	38 (17)	40.5 ± 10	pre	42.2 ± 2	(14.8 ± 8)	-	1.6 ± 2	-	7	3
13 Tabrizi et al. 2009 [6][2]	122 (54)	46.1 ± 10	62 (29)	41.1 ± 9	pre	42.2 ± 2	(14.1)	13 ± 0.4	2.2 ± 1	-	3	4
			58 (25)	40.6 ± 9	pre	44.2 ± 3	(8.6)	12.8 ± 1	2.8 ± 2	-	6	4
			73 (31)	46.7 ± 10	I	43.9 ± 3	-	12.3 ± 1	19.1 ± 9	-	55	4
			46 (25)	51.4 ± 9	II	43.5 ± 2	-	8.6 ± 1	30.6 ± 10	-	54	4
14 Thieben et al. 2002 [26]	16 (10)	38 ± 11	18 (9)	43.6 ± 12	pre	41.1 ± 3	-	-	2.23	292.95	10	10
15 Wolf et al. 2007 [17]	16 (11)	36.3 ± 11	16 (9)	35.2 ± 9	pre	42.2 ± 3	(19.7 ± 10)	-	1.6 ± 2	325.5 ± 45	4	8

No. Authors	Control subjects		HD subjects					UHDRS scores			GM foci	FWHM mm
	n (male)	age years	n (male)	age years	HD stage	CAG repeats	DD (YEO) years	TFC	motor	cognitive		
16 Wolf et al. 2009 [27]	16 (11)	36.3 ± 11	12 (9)	48.4 ± 10	I, II	44.8 ± 4	6.6 ± 3	11.6 ± 1	28.3 ± 9	215.9 ± 54	14	8
17 Zimbelman et al. 2007 [28]	12 (3)	31.4 ± 9	13 (5)	34.9 ± 9	pre[4]	48.2 ± 6	(7.9 ± 3)	-	-	-	2	12
Total/mean ± SD	507 (229)	42 ± 6	685 (319)	44 ± 6		43.8 ± 2		11.2 ± 2	17.7 ± 14	247 ± 51	318	

Values represent numbers of subjects or means ± SD, as appropriate and if not indicated otherwise. HD stage is recorded as pre-HD (pre), symp-HD (symp) or symptomatic stages I, II or III according to the classification of Shoulson and Fahn [29]. DD = Disease duration; YEO = years to estimated onset based on current age and CAG repeats (Langbehn et al. [40]); TFC = total functional capacity; GM = gray matter; FWHM = isotropic Gaussian smoothing kernel (full width at half maximum).

[1] Subset of the PREDICT-HD sample.

[2] TRACK-HD sample.

[3] This study also comprised a group of pre-HD subjects, but since VBM analysis did not reveal any significant differences between the control and pre-HD group, this contrast could not be included in the meta-analysis.

[4] Only the subgroup ‘close’ to estimated disease onset was included, which showed differences in gray matter volume compared to controls, whereas the ‘far’ group did not.

Table 2

Significant clusters of convergence in the ALE meta-analyses

Cluster No.	Volume mm^3	MNI coordinates[1]			Lat.	Macroanatomical and cytoarchitectonic region	Contributing studies[2]
		x	y	z			
Pre-HD studies							
Cluster 1	13,208	26	8	8	R	caudate nucleus; putamen; pallidum; amygdala (CM, LB); hippocampus (CA); insula	8, 13b, 5, 13a, 15, 1, 9, 14, 7, 11, 6, 13c, d
Cluster 2	10,272	−14	6	14	L	caudate nucleus; putamen; thalamus	1, 11, 8, 9, 14, 6, 7
Cluster 3	2,048	30	−72	28	R	middle occipital gyrus; superior occipital gyrus	8, 14, 10
Cluster 4	1,496	−32	−12	−8	L	putamen; amygdala (CM, LB); hippocampus (CA)	13b, 14
Symp-HD studies							
Cluster 1	6,344	24	6	10	R	caudate nucleus; putamen; pallidum; nucleus accumbens	6, 11, 5, 13c, d
Cluster 2	5,144	−10	12	8	L	caudate nucleus; putamen; pallidum	6, 9, 14, 4
Cluster 3	3,128	−34	−28	52	L	precentral gyrus, M1 (BA 4p, 4a); postcentral gyrus, SI (BA 3b, 3a, 2); inferior parietal cortex (PFt); intraparietal sulcus (hIP1; hIP2; hIP3)	13c, 4, 13d, 1, 10
Cluster 4	1,960	10	−12	46	R	middle cingulate cortex; medial PMC, SMA (BA 6)	13d, 13c
Cluster 5	1,904	40	2	38	R	inferior frontal gyrus (BA 44); middle frontal gyrus; precentral gyrus	13c, 13d, 9
Cluster 6	1,848	−42	8	28	L	inferior frontal gyrus (BA 44); middle frontal gyrus; precentral gyrus	13c, 4, 13d, 9
Cluster 7	1,808	−54	−8	6	L	parietal operculum, SII (OP4); Heschl's gyrus, PAC (TE 1.2, 1.0); insula	13c, 13d, 5, 4, 1, 9
Cluster 8	1,496	34	−24	52	R	precentral gyrus, M1 (BA 4p, 4a), PMC (BA 6)	13d, c, 1, 10
All HD studies							
Cluster 1	6,880	−12	12	6	L	caudate nucleus; putamen; pallidum	9, 6, 14
Cluster 2	5,872	24	8	8	R	caudate nucleus; putamen; pallidum	6, 7, 11, 13b, d
Cluster 3	4,056	−48	10	37	L	inferior frontal gyrus (BA 44, 45); middle frontal gyrus; precentral gyrus	4, 9, 13c, 3, 2, 13d, 1
Cluster 4	3,824	−48	−12	46	L	precentral gyrus, M1 (BA 4a, 4p), PMC (BA 6); postcentral gyrus, SI (BA 3b, 3a, 1, 2); inferior parietal cortex (PFt); intraparietal sulcus (hIP2; hIP3)	13c, 13d, 9, 4, 1, 10
Cluster 5	2,872	40	4	38	R	inferior frontal gyrus (BA 44); middle frontal gyrus; precentral gyrus	9, 13c, 13d
Cluster 6	2,280	−26	−80	20	L	middle occipital gyrus; superior occipital gyrus; cuneus; precuneus	13d, 9, 13c, 4, 10
Conjunction: pre-HD and symp-HD							
Cluster 1	4,816	−12	12	8	L	caudate nucleus; putamen; pallidum	
Cluster 2	3,976	24	6	10	R	caudate nucleus; putamen; pallidum	
Contrast: symp-HD > pre-HD							

Cluster No.	Volume mm^3	MNI coordinates[1]			Lat.	Macroanatomical and cytoarchitectonic region	Contributing studies[2]
		x	y	z			
Cluster 1	4,872	−36	−26	50	L	precentral gyrus, M1 (BA 4p, 4a), PMC (BA 6); postcentral gyrus, SI (BA 3b, 3a, 1, 2); inferior parietal cortex (PFt); intraparietal sulcus (hIP1; hIP2; hIP3)	
Cluster 2	2,240	8	8	4	R	caudate nucleus; putamen; pallidum; nucleus accumbens	
Cluster 3	1,808	−56	−10	6	L	parietal operculum, SII (OP4); Heschl's gyrus, PAC (TE 1.2, 1.0); insula	
Cluster 4	1,496	34	−24	52	R	precentral gyrus, M1 (BA 4p, 4a), PMC (BA 6)	
Cluster 5	1,016	46	0	38	R	inferior frontal gyrus (BA 44); middle frontal gyrus; precentral gyrus	
Cluster 6	824	−44	6	42	L	inferior frontal gyrus (BA 44); precentral gyrus	
Cluster 7	760	12	−12	48	R	middle cingulate cortex; medial PMC, SMA (BA 6)	
Cluster 8	608	−28	−78	18	L	middle occipital gyrus; superior occipital gyrus	
Cluster 9	400	−10	−56	30	L	precuneus; cuneus	

Lat. = Laterality; L = left; R = right; PAC = primary auditory cortex; CM = centromedial; LB = laterobasal; CA = cornu ammonis; BA = Brodmann area.

[1] Montreal Neurological Institute (MNI) coordinates (x, y, z) for the maximum ALE value.

[2] Numbers of the studies (from table 1) contributing to the cluster (only studies with a contribution probability of $p > 0.30$ are mentioned; order indicates decreasing probability).

Table 3

Significant clusters of convergence in the ALE correlation analysis

Cluster No.	Volume mm^3	MNI coordinates[1]			Lat.	Macroanatomical and cytoarchitectonic region	r_s
		x	y	z			
CAG repeat length							
Cluster 1	2,576	12	11	6	R	caudate nucleus; putamen; nucleus accumbens	0.54
Age							
Cluster 1	2,080	−39	−27	46	L	precentral gyrus, Ml (BA 4p, 4a); postcentral gyrus, SI (BA 3b, 3a, 2); inferior parietal cortex (PFt); intraparietal sulcus (hIP2)	0.53
Cluster 2	1,512	4	14	−4	R	caudate nucleus; putamen	0.51
Cluster 3	1,488	36	−24	46	R	precentral gyrus, M1 (BA 4p, 4a), PMC (BA 6)	0.56
Cluster 4	1,144	−52	−10	0	L	parietal operculum, SII (OP4); Heschl's gyrus, PAC (TE 1.2, 1.0)	0.49
Cluster 5	200	−10	16	0	L	caudate nucleus; putamen	0.47
Estimated disease burden							
Cluster 1	3,216	8	14	−6	R	caudate nucleus; putamen; pallidum; nucleus accumbens	0.62
Cluster 2	1,416	36	−24	46	R	precentral gyrus, M1 (BA 4p, 4a), PMC (BA 6)	0.49
Cluster 3	992	−42	−34	38	L	precentral gyrus, M1 (BA 4p); postcentral gyrus, SI (BA 3b, 3a, 2); inferior parietal cortex (PFt)	0.48
Estimated disease progression							
Cluster 1	1,416	36	−24	46	R	precentral gyrus, M1 (BA 4p, 4a), PMC (BA 6)	0.54
Cluster 2	1,056	−6	8	0	L	caudate nucleus	0.55
Cluster 3	600	−40	−30	40	L	precentral gyrus, M1 (BA 4p); postcentral gyrus, SI (BA 3b, 3a, 2)	0.55
UHDRS motor score							
Cluster 1	2,040	−39	−27	46	L	precentral gyrus, M1 (BA 4p, 4a); postcentral gyrus, SI (BA 3b, 3a, 2); inferior parietal cortex (PFt); intraparietal sulcus (hIP2)	0.52
Cluster 2	1,496	36	−24	46	R	precentral gyrus, M1 (BA 4p, 4a), PMC (BA 6)	0.56
Cluster 3	1,072	12	4	5	R	caudate nucleus	0.51
Cluster 4	424	−52	−8	0	L	parietal operculum, SII (OP4); Heschl's gyrus, PAC (TE 1.2, 1.0)	0.47

Lat. = Laterality; L = left; R = right; r_S = Spearman's rank correlation coefficient; PAC = primary auditory cortex; BA = Brodmann area.

[1] Montreal Neurological Institute (MNI) coordinates (x, y, z) for the maximum ALE value.